blood advances

American Society of Hematology
2021 L Street NW, Suite 900,
Washington, DC 20036
Phone: 202-776-0544 | Fax 202-776-0545
bloodadvances@hematology.org

SARS-CoV-2 infection modifies the transcriptome of the megakaryocytes in the bone marrow

Tracking no: ADV-2023-012367R1

Isabelle Allaeys (CRCHU de Quebec-Universite Laval, Canada) Guillaume Lemaire (CHU de Québec, Canada) Mickael Leclercq (Centre de Recherche du Centre Hospitalier Universitaire de Québec, Canada) Emile Lacasse (CHU de Quebec, Canada) Maude Fleury (CHU de Québec, Canada) Isabelle Dubuc (CHU de Quebec, Canada) Leslie Gudimard (CHU de Québec, Canada) Florian Puhm (Centre de Recherche du Centre Hospitalier Universitaire de Québec, France) Julia Tilburg (Boston Childrens Hospital and Harvard Medical School, United States) Andrew Stone (Harvard Medical School and Boston Children's Hospital, United States) Kellie Machlus (Harvard Medical School and Boston Children's Hospital, United States) Arnaud Droit (Centre de recherche du CHU de Québec, Canada) Louis Flamand (CHU de Quebec Research centre, Canada) Eric Boilard (CHU de Quebec, Canada)

Abstract:
Megakaryocytes, integral to platelet production, predominantly reside in the bone marrow and undergo regulated fragmentation within sinusoid vessels to release platelets into the bloodstream. Inflammatory states and infections influence megakaryocyte transcription, potentially affecting platelet functionality. Notably, COVID-19 has been associated with altered platelet transcriptomes. In this study, we investigated the hypothesis that SARS-CoV-2 infection could impact the transcriptome of bone marrow megakaryocytes. Utilizing spatial transcriptomics to discriminate subpopulations of megakaryocytes based on proximity to bone marrow sinusoids, we identified approximately 19,000 genes in megakaryocytes. Machine learning techniques revealed that the transcriptome of healthy murine bone marrow megakaryocytes exhibited minimal differences based on proximity to sinusoid vessels. Further, at peak SARS-CoV-2 viremia, when the disease primarily affected the lungs, megakaryocytes were not significantly different from those from healthy mice. Conversely, a significant divergence in the megakaryocyte transcriptome was observed during systemic inflammation, although SARS-CoV-2 RNA was never detected in bone marrow and it was no longer detectable in the lungs. Under these conditions, the megakaryocyte transcriptional landscape was enriched in pathways associated with histone modifications, megakaryocyte differentiation, NETosis, and autoimmunity, which could not be explained by cell proximity to sinusoid vessels. Notably, the type-I interferon signature and calprotectin (S100A8/A9) were not induced in megakaryocytes under any condition. However, inflammatory cytokines induced in the blood and lungs of COVID-19 mice were different from those found in the bone marrow, suggesting a discriminating impact of inflammation on this specific subset of cells. Collectively, our data indicate that a new population of bone marrow megakaryocytes may emerge through COVID-19-related pathogenesis.

Conflict of interest: No COI declared

COI notes:

Preprint server: No;

Author contributions and disclosures: .A., L.F., and E.B. conceived and designed the experiments. M.L., A.D., K.R.M., A.S., J.T. and L.F. contributed critical reagent, resources, and expertise. Experiments were performed by I.A., M.F., E.L., I.D., L.G., J.T. and A.S. Data were processed and analyzed by I.A., G.L., M.F. and E.L. and supervised by E.B., M.L., A.D. and L.F. The manuscript was written by I.A. and E.B. and critically reviewed by all authors. Competing interests: The authors declare that they have no competing interest. Data and materials availability: Data associated with this study are present in the paper, the Supplementary Materials or available from the corresponding author on reasonable request.

Non-author contributions and disclosures: No;

Agreement to Share Publication-Related Data and Data Sharing Statement: All sequencing data will be made available on an online repository platform dbgap https://www.ncbi.nlm.nih.gov/gap/docs/submissionguide/ BioProject ID:PRJNA1090478

Clinical trial registration information (if any):

SARS-CoV-2 infection modifies the transcriptome of the megakaryocytes in the bone marrow

Isabelle Allaeys[1,2], Guillaume Lemaire[1,2], Mickaël Leclercq[1,2], Emile Lacasse[1,2], Maude Fleury[1,2], Isabelle Dubuc[1,2], Leslie Gudimard[1,2], Florian Puhm[1,2], Julia Tilburg[3], Andrew Stone[3], Kellie R. Machlus[3], Arnaud Droit[1,2], Louis Flamand[1,2] and Eric Boilard[1,2]

[1] Centre de Recherche du Centre Hospitalier Universitaire de Québec - Université Laval, Québec, QC, Canada
[2] Centre de Recherche ARThrite - Arthrite, Recherche, Traitements, Université Laval, Québec, QC, Canada.
[3] Vascular Biology Program, Boston Children's Hospital and Department of Surgery, Harvard Medical School, Boston, MA, USA.

Correspondence should be sent to:

Eric Boilard, PhD.
Centre de Recherche du Centre Hospitalier Universitaire de Québec
Faculté de Médecine de l'Université Laval
2705 Laurier Blvd, room T1-49, Québec, QC, Canada G1V 4G2
Eric.Boilard@crchudequebec.ulaval.ca
Phone: +1 418-525-4444, extension 46175, Fax: +1 418-654-2765

Data availability
The datasets generated and/or analyzed during the current study are available from the corresponding author on reasonable request subject to ethics approval. All sequencing data will be made available on an online repository platform dbgap https://www.ncbi.nlm.nih.gov/gap/docs/submissionguide/ BioProject ID:PRJNA1090478

COI: The authors have no COI to disclose

Key Points

1) In a mouse model of SARS-CoV-2 infection, cytokines in the bone marrow are different from those in blood and lungs
2) SARS-CoV-2-mediated inflammation promotes changes to the megakaryocyte transcriptome in the bone marrow

Abstract

Megakaryocytes, integral to platelet production, predominantly reside in the bone marrow and undergo regulated fragmentation within sinusoid vessels to release platelets into the bloodstream. Inflammatory states and infections influence megakaryocyte transcription, potentially affecting platelet functionality. Notably, COVID-19 has been associated with altered platelet transcriptomes. In this study, we investigated the hypothesis that SARS-CoV-2 infection could impact the transcriptome of bone marrow megakaryocytes. Utilizing spatial transcriptomics to discriminate subpopulations of megakaryocytes based on proximity to bone marrow sinusoids, we identified approximately 19,000 genes in megakaryocytes. Machine learning techniques revealed that the transcriptome of healthy murine bone marrow megakaryocytes exhibited minimal differences based on proximity to sinusoid vessels. Further, at peak SARS-CoV-2 viremia, when the disease primarily affected the lungs, megakaryocytes were not significantly different from those from healthy mice. Conversely, a significant divergence in the megakaryocyte transcriptome was observed during systemic inflammation, although SARS-CoV-2 RNA was never detected in bone marrow and it was no longer detectable in the lungs. Under these conditions, the megakaryocyte transcriptional landscape was enriched in pathways associated with histone modifications, megakaryocyte differentiation, NETosis, and autoimmunity, which could not be explained by cell proximity to sinusoid vessels. Notably, the type-I interferon signature and calprotectin (S100A8/A9) were not induced in megakaryocytes under any condition. However, inflammatory cytokines induced in the blood and lungs of COVID-19 mice were different from those found in the bone marrow, suggesting a discriminating impact of inflammation on this specific subset of cells. Collectively, our data indicate that a new population of bone marrow megakaryocytes may emerge through COVID-19-related pathogenesis.

Introduction

Megakaryocytes reside primarily in the bone marrow where they derive from the myeloid branch of hematopoiesis. They are rare (<0.05% of the bone marrow cellular population), and recognizable due to their large size (up to 100 µm), polyploid nucleus and expression of surface glycoproteins (e.g., IIb and IIIa of the IIb/IIIa complex). Through several rounds of DNA replication without cellular division and an intricate maturation process, megakaryocytes generate proplatelets, which protrude into blood sinusoids and fragment into anucleate platelets.[1-3] Thus, megakaryocytes are the cellular precursors of platelets, whose RNA content (coding and non-coding) mirrors that of the mother megakaryocytes.

Megakaryocytes help maintain hemostasis through their prominent role in platelet production; however, evidence suggests that they also regulate other functions. They support the hematopoietic stem cell niche by producing cytokines and chemokines (PF4, TGF-b, FGF1, and IGF1).[2,4-6] Their role in immunity is suggested by the expression of immune receptors, including Toll-like receptors that recognize pathogen-associated molecular patterns, receptors capable of direct recognition of pathogens (e.g. CLEC-2, GPVI), and Fc receptors that can bind antibody-coated antigens, and they can present antigens and promote T-cell proliferation.[7-12] Furthermore, megakaryocytes express receptors for cytokines, such as interferon (IFN), interleukin (IL)-1, IL6, TNF and RANTES.[7,8,13,14]

The study of the platelet transcriptome confirms that gene expression is regulated in megakaryocytes during inflammation or infection.[15] During sepsis as well as in the murine cecal ligation and puncture model human and murine platelets, respectively, show hundreds of altered genes, including enhanced expression of *ITGA2B* (glycoprotein IIb encoding gene).[16] In Dengue and Influenza virus infection, platelets are enriched in IFN-stimulated genes such as *IFTIM3,*[17] while platelets in patients with systemic lupus erythematosus (SLE) and in murine models of SLE also show enhanced expression of IFN-stimulated genes,[18-20] thus pointing to a common role of IFN in megakaryocyte functions in both viral infection and autoimmune disease.

Megakaryocytes are a heterogenous population of cells that vary notably in terms of ploidy and size.[2] Recent single-cell transcriptomic analyses revealed that distinct subpopulations of megakaryocytes exist in the bone marrow, each with potentially different specialized functions. Clustering of megakaryocytes on the basis of transcript enrichment identified four main subpopulations of megakaryocytes related to: (1) "*cell cycling,*" (2) "*platelet generation,*" (3) "the *hematopoietic stem cell niche,*" and the more rare (4) "*inflammation."* [2,21,22] While the "*platelet generation*"-related megakaryocytes are suggested to be found near bone marrow sinusoids, the injection of lipopolysaccharide in mice led to stimulation and expansion of "*inflammation"*-related megakaryocytes located farther from blood vessels.[21] Cellular heterogeneity can also result from organ

distribution. Megakaryocytes are found in lungs,[23-25] where they also generate platelets, and may have a privileged access to allergens, microbiota and infectious agents. Single-cell transcriptomic analyses shed light on distinct populations of megakaryocytes such as those with an immune phenotype in lungs, as well as in the spleen under conditions of sepsis.[24-26]

The severe acute respiratory syndrome coronavirus 2 (SARS-CoV-2) is a highly contagious virus that causes COVID-19. Although manifestations and severity of the disease vary between infected individuals, millions of lives were lost due to COVID-19. The virus mainly affects the lungs, which can cause severe respiratory complications and hypoxia. Systemic inflammation can occur even after the virus is largely eliminated from the lungs due to the cytokine storm that sometimes accompanies the disease. Enhanced coagulopathy and thrombosis are observed in COVID-19 patients,[27,28] and studies performed at the onset of the pandemic rapidly reported the increased platelet activation and presence of IFN-stimulated gene signature in platelets.[29-31] Furthermore, single-cell RNA sequencing analyses of cells in the blood circulation of patients with COVID-19 identified a subset of megakaryocytes with altered gene transcription, such as enhanced IFN-stimulated genes, major histocompatibility complex (MHC)-II and calprotectin (S100A8/A9),[32,33] pointing to effects of SARS-CoV-2 or the dysregulated inflammatory response on megakaryocyte transcription.

Localized near the sinusoids where they are ready to release their platelets, megakaryocytes may be more likely to sense inflammatory mediators from the blood circulation. We hypothesized that the systemic inflammation prevalent in SARS-CoV-2 infection would affect the transcriptome of the bone marrow megakaryocytes, principally those with direct access to blood. To verify this, we used a spatial transcriptomic approach to examine megakaryocytes at different stages of pathogenesis.

Methods

Additional details can be found as supplementary material.

Mice

All animal experiments were conducted under biosafety level 3 confinement and approved by the Université Laval animal committee (#2021-90). B6.Cg-Tg(K18-hACE2)2Prlmn/J (stock#3034860) (K18-ACE2 mice) mice were purchased from the Jackson Laboratories (Bar Harbor, ME, USA). Nine-week to ten-week-old male and female mice were infected with 25µL of medium containing 250 or 500 ($TCID_{50}$) of SARS-CoV-2 or 25µL of medium for mock-infected mice. Mouse body temperature and weight were recorded every day for 10 days. Mice (19.55 ± 2.95 grams at Day 0) were euthanized when a weight-loss threshold of 20% was reached. On day 3 and 7, mice (n=5/group) were euthanized, and lungs collected for assessment of viral loads, RNA extraction, tissue homogenization for cytokine analysis and histological studies. Bone marrow cells and bone marrow plasma were obtained by flushing one femur in 300ul of PBS containing 2mM EDTA and

cells were spun down 5 min at 300g at room temperature. Supernatant was considered as bone marrow plasma and cell pellet was used to extract RNA.

Immunofluorescence

Femurs and lung were harvested, fixed for 24 hours in 10% buffered formalin at 4°C and femur were decalcified for 14 days in 14% EDTA at 4°C. Lung or decalcified bones were saturated 24 hours in PBS containing 30% sucrose at 4°C and cryopreserved in M-1 embedding matrix (Epredia^{TM}). Staining was performed on 6 µm cryosections using 1 µg/mL of rabbit anti-CD41 (EPR17876, Abcam) or 25 µg/mL of rabbit anti-N (Rockland Immunochemicals Inc.) and counterstain with Hoechst 33342 (10 µg/mL, Thermofisher). AF488-goat anti-rabbit (2µg/mL, Thermofisher) was used as secondary antibody. Tissue autofluorescence was quench for 3 minutes using TrueVIEW Autofluorecence Quenching kit (Vector Laboratories). Sections were mounted using VECTASHIELD Vibrance Antifade Mounting Medium (Vector Laboratories). For quantification, images were acquired at 20x with a slide scanner (Zeiss Axio Scan.Z1) connected to a Colibri 2 camera (Zeiss, Germany). CD41 positive cells (MK) and SARS-CoV2 covering surfaces were quantified using a total surface of at least 1.5 mm^2, randomly assigned and using Zen 3.3 software and imageJ. Megakaryocyte mean size and mean area were quantified using 70 cells randomly assigned and frequency distribution was calculated. Representative images were acquired using a Z2 confocal microscope with LSM 800 scanning system (Zeiss, Germany). Images were captured with a 20x objective. The mean size of all megakaryocytes located in the region of interest (ROI) and captured for the transcriptomic analyzes was evaluated using Fiji.

Immunohistology

Lungs were fixed 24h in 10% neutral buffered formaldehyde solution, embedded in paraffin, and sectioned. The 5-µm thick sections were stained with a modified Carstairs' method to distinguish platelets and fibrin in histological sections: platelet thrombi (grey), fibrin (orange-red), red blood cells (orange-yellow), and collagen (bright blue).[34,35] A histologic scoring index was developed to evaluate lung damage using presence of platelet thrombi (0 to 3) and cell infiltration (0 to 3).

GeoMx digital spatial profiling (DSP) for whole transcriptome analysis

Femurs from female K18-hACE2 mice infected with SARS-CoV2 (500 $TCID_{50}$) for 3 (COVID_3d) or 7 days (COVID_7d) or with conditioned media (Mock) for 7 days were fixed in formalin 24h, decalcified 14 days with EDTA and embedded in paraffin. 10 µm sections were prepared and mounted onto Leica Bond Plus microscope slides. Digital Spatial Profiling was performed by NanoString Technologies using the GeoMX platform with the Nanostring Mouse Whole Transcriptome Atlas. Immunofluorescence staining was performed using anti-CD41 (EPR17876, Abcam) and anti-endomucin (clone V.7C7, SantaCruz Biotechnology) as morphological markers along with Syto13 DNA nucleic acid

staining, in order to design region of interest (ROI). ROI were selected based on the fluorescence of interest (CD41) and whether Megakaryocytes (MK) were adjacent to sinusoid vessels (ASV-MK) or non-adjacent to sinusoid vessels (NASV-MK). Oligos from the hybridized probes were released by photo-cleaving UV light (385 nm). Sequencing libraries were constructed and subsequent sequencing and counting were performed on an Illumina NovaSeq6000 and fastq files were processed by the NanoString DND pipeline, resulting in count data for each target probe in each ROI. LOQ (Limit of Quantitation) was set to detect gene outliers. The limit was defined by the geometric mean of the negative probes multiplied by the square of geometric standard deviations of the negative probes, as generally recommended by the manufacturer. The data for each ROI were adjusted to achieve the same 75th percentile (Q3) of RNA expression signal using a normalization strategy generally used for whole transcriptome data analysis.[36] 19,072 genes normalized by 3rd quartile (Q3) were expressed above LOQ (Limit of Quantitation) in at least 10% of ROI. Differentially expressed genes between ROIs and conditions were selected on the basis of statistically significant differences (FDR adjusted P-value < 0.05 and an absolute $\log_2$ fold-change >1).

Bioinformatic analyses

Gene expression data normalized by 3rd quartile were retrieved from the Nanostring platform. We then identified gene signatures associated with various comparisons, including COVID at 3 days vs control, and COVID at 7 days vs control. In these conditions, we also compared cells that were adjacent and non-adjacent to sinusoid vessels. Signatures were identified with BioDiscML,[37] a machine learning sequential minimal optimization algorithm designed to identify predictive features within a given condition (Table S1). This tool trains thousands of models using many machine learning classifiers (e.g., Naïve Bayes, Random Forest, SVMs). All models are evaluated by cross validation procedures, (e.g., k-fold, Bootstrapping, repeated holdout) to prevent overfitting, on which standard deviation was calculated. It also performs feature selection using stepwise learning and top-k features based on information gain ranking. Furthermore, since stepwise feature selection tends to remove all correlated features, for each “short signature” we retrieved correlated genes using Pearson and Spearman coefficients ≥ 0.9. Finally, we performed a functional analysis of the signatures using g:Profiler.[38]

Statistics

Statistical analyses were performed using GraphPad Prism software (v10.0.3). Results are expressed as mean ± standard deviation (SD). p-values (P) <0.05 were considered statistically significant.

Biorender (https://www.biorender.com/) was used to draw schematics (Figure 1A and Figure 3A) and the graphical abstract.

All animal experiments were conducted under biosafety level 3 confinement and approved by the Universit Laval animal committee (2021-90).

Results

SARS-CoV-2 infection in mice stimulates the production of cytokines in the bone marrow that differ from those found in the blood and lungs

SARS-CoV-2 requires interaction between viral Spike (S) protein and its counterreceptor, the human angiotensin I converting enzyme-2 (ACE2), to gain cell entry. Given that SARS-CoV-2 protein S does not bind murine ACE2, we utilized transgenic mice that expressed human ACE2 under the control of the human keratin 18 promoter (K18-hACE2 transgenic mice).[39] Mice housed in a NC3 respiratory facility were either intranasally injected with diluent, or with SARS-CoV-2 Delta variant [250 tissue culture infectious dose 50 (TCID50)]. In these experimental conditions, infected mice showed robust lung viral loads at Day 3, and gradually showed signs of severe pathogenesis, as assessed by weight loss and a moribund appearance, until Day 7 when the manifestations were the most severe (**Figure 1A–D**). By Day 7, the mice had largely eliminated SARS-CoV-2 infectious particles from the lungs, but were affected by systemic inflammation (**Figure 1 D, E**), as expected in this established model.

SARS-CoV-2 infection increases the lung cytokine load, such as IL-6, TNF and chemokines, in both humans and mice.[40,41] To identify cytokines in the bone marrow and to determine whether they resembled those in the blood or the lungs, we collected bone marrow from the murine femurs, from which we isolated the plasma after eliminating the marrow cells by centrifugation. We screened for the presence of 33 cytokines and chemokines in bone marrow plasma from uninfected mice and SARS-CoV-2-infected mice at Days 3 and 7, and compared these with autologous blood plasma and lung homogenates. As expected, several cytokines were detected in blood plasma and lungs, both at Day 3 and Day 7 of infection (**Figures 1E**). Interestingly, as the disease developed, cytokines were differentially regulated in the bone marrow compared to blood plasma or lung (**Figure 1E, S1–S3**). For instance, platelet factor 4 (PF4), which increases in the blood of COVID-19 patients,[41] was also increased in the blood of mice after 3 days of infection while its levels decreased in lungs (**Figure 1E**). Calprotectins (S100A8/A9) increase in circulating megakaryocytes and platelets in humans with COVID-19,[32,33,42] but were reduced in bone marrow plasma (**Figure 1E**), potentially due to emergency hematopoiesis and the egress of granulocytes. IFN-γ, which would promote the expression of IFN-stimulated genes in platelets in COVID-19 patients,[30] increased in blood and lungs but remained unchanged in the bone marrow (**Figure 1E**). In contrast, IL-9 and IL-15 levels increased in the bone marrow, while it remained unchanged in the other locations studied (**Figure 1E**). The striking occurrence of a cytokine gradient in blood relative to the bone marrow compartment prompted us to examine the

transcriptome of bone marrow megakaryocytes closely, and to compare megakaryocytes distant from sinusoid vessels to those directly adjacent to blood vessels, as the latter may be more likely to be influenced by circulating inflammatory factors released in response to viral infection.

Use of spatial transcriptomics to examine bone marrow megakaryocytes

We first characterized the bone marrow in terms of megakaryocyte density and occurrence during SARS-CoV-2 infection. We observed an average of 75 megakaryocytes per mm^{-2} in the uninfected mice, a number which gradually decreased through the course of the disease, falling by 50% at 7 Days post infection (**Figure 2A, B**). Despite a decrease in the number of megakaryocytes in the bone marrow, the platelet count remained unchanged during infection at all the examined time points (**Figure S4**). Further, the frequency distribution of megakaryocyte size and area remained unaltered during infection (**Figure 2C**). Although SARS-CoV-2 was easily detected in the lungs of infected mice, the virus was not detected in the bone marrow at any of the time points studied, using either antibodies directed against the nucleocapsid protein N or PCR to detect the viral genome (**Figure 2D, E**). These observations suggest that SARS-CoV-2 does not reach the bone marrow at any of the time points studied.

We used spatial transcriptomics to assess the transcriptomes of cells in situ (**Figure 3A**). Megakaryocytes in paraformaldehyde-fixed femurs were identified by their characteristic size (mean size in µm ± SD, Mock: 22.91 ±5.243 (n=90), 3 days: 23.07 ±5.302 (n=90), 7 days: 24.72 ±5.513 (n=71)), nuclear staining, and CD41 surface expression, while blood vessels were identified by using the endomucin marker. Previous work that employed a similar spatial transcriptomic approach to study bone marrow megakaryocytes in healthy mice showed that as many as 1,000 gene transcripts could be identified by the capture of a single megakaryocyte.[43] To enhance the power of downstream analyses, we determined the transcriptome of 8–10 megakaryocytes directly adjacent to sinusoid vessels (ASV), and compared this to equivalent number of megakaryocytes non-adjacent to sinusoid vessels (Non-ASV). We then replicated these analyses in 6 distinct areas each (**Figure 3A, B**). Using this approach, a total of 19,072 genes were identified from all conditions using this approach.

The transcriptome of bone marrow megakaryocytes is altered in COVID-19

We first evaluated the overall impact of infection on megakaryocyte transcription, irrespective of the megakaryocyte localization within the bone marrow. By Day 3 of infection, a total of 32 and 1466 transcripts were significantly up- and down-regulated, respectively (**Figure 3C**). The use of machine learning to identify a minimal signature did not generate a reliable signature. Principal component analysis (PCA) and Uniform Manifold Approximation and Projection (UMAP) on the obtained signature failed to exhibit clean separation, and although the

Matthew's Correlation Coefficient (MCC=0.915) was high, the elevated standard deviation (SD=0.095) prevented to confidently identify the presence of a gene signature that would efficiently distinguish the two megakaryocyte populations (**Figure S5**). However, pathogenesis had more segregating effects on the megakaryocyte transcriptome by Day 7, as 28 genes were up-regulated and 1291 genes were down-regulated at this timepoint (**Figure 3D**). In addition to the UMAP separation on all genes of the two conditions (**Figure S6A**), a short predictive signature derived from the machine learning analyses contained 30 gene transcripts (MCC and SD; 0.997; 0.008), among which numerous genes had statistically significant differences (**Figure S6B**) that could efficiently distinguish the two populations of megakaryocytes (**Figure 3E**). Gene ontology (GO) and KEGG enrichment analyses determined that pathways relating to biological processes such as histone modifications, megakaryocyte differentiation, NETosis, COVID-19 and systemic lupus erythematosus were impacted in megakaryocytes in the COVID-19-infected mice (**Figure 3F, G**). PF4, identified by the signature and generally considered to be specifically expressed in the bone marrow by megakaryocytes, was confirmed to decrease after 7 days of infection in an independent cohort of mice treated with the same experimental conditions (**Figure 3H**), further validating our spatial transcriptomic analyses. Notably, IFN-stimulated genes were not modulated in megakaryocytes (**Figure S7A**), which may be explained by the absence of IFN increase (**Figure 1F**) and SARS-CoV-2 (**Figure 2D, E**) in the bone marrow. Moreover, calprotectin levels, which increase in circulating megakaryocytes in humans with COVID-19,[32] was not altered in megakaryocytes in the bone marrow (**Figure S7B)**. Thus, in the murine model of lung infection by SARS-CoV-2, there were significant and unique alterations to the transcriptome of bone marrow megakaryocytes.

While selecting megakaryocytes to process for transcriptome analyses, we selected a balanced number of megakaryocytes that were either adjacent (ASV) or non-adjacent (Non-ASV) to the marrow sinusoids. We thus aimed to verify whether megakaryocyte localization within the bone marrow was a factor that could influence the overall transcription pattern. We identified 528 differently expressed genes in healthy mice (**Figure 4A**). UMAP plot did not distinguish the 2 populations of megakaryocytes (**Figure 4B**), and machine learning analyses failed to generate a model capable of accurately predicting megakaryocyte localization (MCC = 0.769 (SD = 0.186)) in absence of disease (**Figure S8**), suggesting that the spatial localization of the megakaryocytes relative to sinusoid vessels has no or only a limited impact on megakaryocyte transcriptomes under healthy conditions.

Given the effects of SARS-CoV-2 on megakaryocytes 7 days post-infection, we examined at this time point whether the pathogenesis would preferentially alter megakaryocytes in a specific location relatively to bone marrow sinusoids. Infection led to the respective up- and down-regulation of 83 and 1,084 genes in

ASV megakaryocytes (**Figure 4C**), while 40 and 747 were up- and down-regulated in Non-ASV megakaryocytes (**Figure 4E**). Non-ASV and ASV megakaryocytes from healthy and Day 7 COVID-19 mice were distinguished by machine learning with a 15-gene signature that sufficed to specifically identify ASV megakaryocytes (**Figure 4D, F-H**), although a high SD was measured due to the presence of outliers (MCC = 0.922 (SD = 0.113)). A longer 30-gene signature was needed for the Non-ASV megakaryocytes (MCC=0.922 (SD=0.114)), which is attributable to model overfitting and pointing to the absence of significant difference between cells in this location. GO and KEGG enrichment analyses using both signatures highlighted pathways such as histone modifications, megakaryocyte differentiation, NETosis, and systemic lupus erythematosus, both in ASV and Non-ASV megakaryocytes (**Figure S9**). As these results are reminiscent of those found in comparisons that did not take into account position relative to sinusoid vessels, it suggests that most of the enriched pathways occur in megakaryocytes irrespectively of their location.

Discussion

COVID-19 patients have higher risk of thrombosis[27,28] and postmortem investigations as well as intravital imaging in SARS-CoV-2 infected K18-hACE2 transgenic mice revealed platelet thrombi in lung and brain vasculature.[40,44] Given the alterations to the platelet transcriptome in COVID-19 patients,[30,42] which may give rise to hyperactivated platelets,[29-31,45] we aimed to determine whether megakaryocytes in the bone marrow were capable of sensing the disease and thereby modifying their transcriptome. Using a murine model of SARS-CoV-2 infection, we identified a set of cytokines and chemokines that are differentially expressed in bone marrow versus the blood and lungs at different stages of the disease. We show that the megakaryocyte transcriptomic landscape is profoundly impacted at the time of systemic inflammation, when the virus is essentially cleared from the lungs and is absent in bone marrow. Moreover, we suggest that the spatial localization of the cells within the marrow is not a variable that would impact megakaryocyte transcriptomic alterations in this disease.

Respiratory tract infections are highly contagious and are responsible of millions of deaths worldwide each year, often following seasonal cycles. During Influenza or Sendai virus infection, type-I IFN produced in the lungs can affect cells in the bone marrow,[46] thereby driving anti-viral responses in emerging immune cells despite the absence of viral particles in the bone marrow. Interleukin (IL)-1 and IL-6, produced during Influenza infection, can also trigger emergency megakaryopoiesis, driving megakaryocyte production directly from CD41-positive (megakaryocyte-committed) hematopoietic stem cells.[47] Megakaryopoiesis, however, was unlikely implicated in COVID-19 mice, as the number of megakaryocytes was reduced by the infection. SARS-CoV-2 primarily infects the host lung epithelium to cause respiratory tract inflammation, although its persistence and distribution in the human body such as in kidneys, testis and

brain varies greatly between individuals.[48-51] We show that megakaryocytes localized in the bone marrow, more specifically in the femur, respond to inflammation through changes to their transcriptome during the course of lung infection. The transcriptional changes are unlikely to be due to SARS-CoV-2 itself, as the virus was mostly eliminated at this time and was undetectable in the bone marrow. IFN was not detected in blood nor was it induced in the bone marrow, and megakaryocytes in bone marrow examined at all stages of the disease never overexpressed IFN-stimulated genes (**Figure S7A**), perhaps due to the low IFN-inducing potential of SARS-CoV-2.[52] It remains to be determined what molecule(s) stimulate(s) megakaryocytes in the bone marrow, but our survey of cytokines in both the bone marrow and blood suggest that cytokines such as RANTES, known to induce proplatelet formation by megakaryocytes, or IL9 and IL15, might be implicated.[53] Damage-associated molecular patterns generated in the pathogenesis,[54] or the reduced levels of S100A8/A9, a trigger of TLR-4, observed in the bone marrow, may also play a role.[55] Moreover, there may be a role for extracellular vesicles, reportedly increased in COVID-19 and capable of reaching megakaryocytes in the bone marrow,[56,57] or lipid mediators of inflammation, also increased in COVID-19.[41] SARS-CoV-2 stimulates tissue factor expression from lung epithelial cells and thrombin activity,[58] which too may activate megakaryocytes[59] and might impact the megakaryocyte transcriptome.

Given the occurrence of both intra- and extra-vascular megakaryocytes in lungs,[25] we cannot rule out that lung megakaryocytes might preferentially interact with SARS-CoV-2. Such interactions may involve ACE2,[60] although its expression in human megakaryocytes is not definitive,[61] or other molecules such as CD147.[62,63] The transcript encoding murine ACE2, which does not interact with SARS-CoV-2, was detected in bone marrow megakaryocytes in our analyses (**Figure S10**). In humans, megakaryocytes in the blood circulation of patients with severe COVID-19 overexpress IFN-stimulated genes and S100A8/9, and contain SARS-CoV-2 RNA and particles.[30,32,64] In our investigation, we did not observe these features in bone marrow megakaryocytes. Although this might be due to intrinsic differences in the pathogenesis between humans and murine models, it may also suggest that a different pool of megakaryocytes from elsewhere than the bone marrow, for example the lungs, makes contact with SARS-CoV-2. These would be the megakaryocytes that generate the platelets containing SARS-CoV-2 (particles and RNA) reported in these patients.[29,30,65,66] Megakaryocytes may also encounter viral particles after they egressed the bone marrow sinusoids, during their transit toward the lung vasculature. Although this is unlikely given the low number of viral particles in blood and the expected short duration of this event, studies suggest that megakaryocytes may potentially repeatedly circulate through the lung vasculature, which may contribute to longer exposure to viral and inflammatory mediators in lungs.[67] In sepsis, there is expansion of the megakaryocyte population in the spleen.[26] Whether this occurs in the murine model is currently unknown.

Valuable information on the occurrence of potential subpopulations of megakaryocytes in bone marrow was provided by recent single-cell RNA sequencing approaches.[21,68] A major challenge in the study of megakaryocytes is maintaining the integrity of these rare cells, and this is even more true for those imbricated in sinusoids as they are less likely to be captured by the harvest of the marrow or to survive the process of single-cell RNA sequencing analysis. This is an issue, as the single-cell RNA sequencing approach depends on cell integrity and excludes apoptotic cells. Moreover, most common, commercial single-cell sequencing approaches (e.g., 10XGenomics, BD Rhapsody) utilize a 10 µm diameter nozzle, suggesting that the larger megakaryocytes may be lost through the process and may be underrepresented. To overcome this, and for safety reasons given the use of virus-infected materials, we examined cells in femurs fixed in paraformaldehyde using Nanostring GeoMx. While conserving the hard-to-get megakaryocytes imbricated in sinusoids, a notable advantage of this sort of analysis is the richness in terms of RNA content of polyploid cells, which would theoretically allow the study of very few megakaryocytes while obtaining sufficient number of RNA molecules for downstream bio-informatic analyses. Little transcriptional changes were found in megakaryocytes at day 3 of infection despite the large viral load at this time and the noticeable changes to cytokine composition in the bone marrow. In contrast, by day 7 we observed numerous changes, attributed by pathways enrichment analyses to histone modifications, megakaryocyte differentiation, NETosis, and autoimmunity. These characteristics may be congruent with changes to subpopulations of megakaryocytes, such as cycling and platelet-producing megakaryocytes. While separating megakaryocytes into the four subclasses on the basis of their transcripts signature identified by Sun et al. (*cell cycling, platelet generation, hematopoietic stem cell niche,* and *inflammatory*),[21] we find that with the exception of *pf4* and *itgb2*, none of the transcript changes composed a particular subclass (**Figure S11**). The data suggest that modifications of histones may favor DNA replication, while megakaryocyte differentiation may result from emergency megakaryopoiesis. As for NETosis, it is reportedly enhanced in COVID-19, while systemic lupus erythematosus shares common features with COVID-19 such as dysregulated immune cells and auto-antibody production. Whether emperipolesis, the process by which neutrophils migrate into megakaryocytes,[69,70] is enhanced in COVID-19 and explains these changes to transcriptome is also a hypothesis to consider. More mechanistic investigations are needed to confirm the role of these megakaryocytes in inflammation and infection.

There are limitations to our study. Human ACE2 expression in K18-hACE2 transgenic mice may not fully replicate its natural distribution in humans. For instance, megakaryocytes may not interact directly with SARS-CoV-2 in these mice, although studies of human platelets suggest that SARS-CoV-2 is internalized despite ACE2 blockade.[65] Tissue immunofluorescence (two-dimensional imaging) has previously been used to define four main subtypes of megakaryocytes, and highlight that both platelet producing- and hematopoietic

stem cell niche- megakaryocytes were localized in the proximity to sinusoid vessels, while immune subpopulations were more distant.[21] Similarly, we used 10-µm thick bone sections in our selection of megakaryocytes relative to sinusoid proximity. However, there might be vessels that were not efficiently visualized and might have been missed due to the 2D imaging approach, as demonstrated elsewhere.[71] We did not identify any impact of sinusoid vessel proximity on megakaryocyte transcriptome in healthy conditions. Even when the mice showed severe signs of disease, direct access of megakaryocytes to blood circulation was not a significant factor, even if a longer gene signature was necessary to segregate Non-ASV megakaryocytes from infected and healthy mice. Although these findings need to be replicated, they are consistent with a very limited intervascular space in the bone marrow and the suggestion that megakaryocytes may thus be vessel-biased in this tissue.[71]

The appreciation of megakaryocyte function in immunity, their diversity in term of subpopulations, and their localization in various organs and tissues motivated broad research. We found that during SARS-CoV-2 infection, particularly during systemic inflammation, the transcriptomic profile of bone marrow megakaryocytes may change. This suggests that the localization of megakaryocytes in the bone marrow does not hinder their response to inflammatory stimuli in COVID-19, even in the absence of persistent infection. Such responsiveness may have implications for their platelet progeny and disease manifestations, as observed in conditions like long-COVID.

Acknowledgements
The authors acknowledge the NanoString team for performing the RNA analysis on the GeoMx DSP platform as part of the TAP program. The work was supported by the Canadian Institutes of Health Research (CIHR) (to EB; LF), the National Institute of Diabetes and Digestive and Kidney Diseases (R03DK124746 to KRM) and the National Heart, Lung, and Blood Institute (R01HL151494 to KRM) at the National Institutes of Health (USA). EB is recipient of an award from the Fonds de Recherche en Santé du Québec.

Author contributions: I.A., L.F., and E.B. conceived and designed the experiments. M.L., A.D., K.R.M., A.S., J.T. and L.F. contributed critical reagent, resources, and expertise. Experiments were performed by I.A., M.F., E.L., I.D., L.G., J.T., F.P. and A.S. Data were processed and analyzed by I.A., G.L., M.F. and E.L. and supervised by E.B., M.L., A.D. and L.F. The manuscript was written by I.A. and E.B. and critically reviewed by all authors. **Competing interests:** The authors declare that they have no competing interest. **Data and materials availability:** Data associated with this study are present in the paper, the Supplementary Materials or available from the corresponding author on reasonable request. All sequencing data will be made available on an online repository platform dbgap https://www.ncbi.nlm.nih.gov/gap/docs/submissionguide/

Figure legends

Graphical Abstract. Spatial Transcriptomic analysis of bone marrow megakaryocytes during SARS-CoV-2 infection. Three days post infection**,** with high pulmonary viremia and inflammation, no significant gene signature was detected in the bone marrow. Seven days post infection, with low pulmonary viremia and high systemic inflammation, a significant gene signature and altered cytokine levels were detected in the bone marrow in absence of virus.

Figure 1. SARS-CoV-2 infection in the K18-hACE2 mouse model. **(A)** Schematic representation of the mouse experimental protocol. K18-hACE2 mice were inoculated intranasally with SARS-CoV-2 (250 $TCID_{50}$) or control media. Tissues (plasma, bone marrow and lung) were collected at 3 and 7 day post-infection (DPI). **(B)** Survival curve of K18-hACE2 mice upon challenge with SARS-CoV-2 (250 $TCID_{50}$, red color) or with control media (Mock, black color). Mortality (endpoint requiring euthanasia) expressed as percentage of survival was monitored every day for 10 days (top panel, n = 17–19 per group). Survival curve statistical analysis was calculated with Log-rank (Mantel-Cox) test, ****$P < 0.0001$. Weight change (bottom panel, n = 4–40) was also reported every day for 10 days and expressed as mean (± SD) percentage of weight at day 0, the average weight before infection was 19.55 ± 2.95 grams. Unpaired t test with Welch correction was used to determine significance (*$p < 0.05$, **$p < 0.01$ and ***$p < 0.001$). **(C)** Lung sections were stained with a Modified Carstairs' method for fibrin and platelets detection: fibrin (bright red), platelets (grey-blue), collagen (bright blue) and red blood cells (orange-yellow). Platelet thrombus (arrow head) and cell infiltration (asterix) are located (scale bar 100 µm). **(D)** Lung damage was evaluated using a histological score (left panel) and lung virus titer (right panel) was quantified at 3 and 7 DPI using lung homogenate on Vero cells and expressed in $TCID_{50}$ per mg of tissue (n = 4–5 per group). Statistics: Mann-Whitney test, *$p < 0.05$. **(E)** Heatmap of cytokine and growth factor profiles in blood plasma (Blood), bone marrow plasma (Bone Marrow) and lung during SARS-CoV2 infection (3DPI, 7DPI or Mock). Cytokine levels (pg mL^{-1}) were subdivided into three groups: 0 to 80 pg mL^{-1} (Low), 0 to 450 pg mL^{-1} (Mid) and 0 to 75,000 pg mL^{-1} (High). The mean concentration for each cytokine is indicated (n = 4–5). Statistics: one-way ANOVA with Dunnett's multiple comparisons (compared to Mock), *$p< 0.05$, **$p< 0.01$, ***$p<0.001$ and ****$p<0.0001$ n=4-5 per group.

Figure 2. Megakaryocyte and SARS-CoV-2 detection in tissue during COVID-19. **(A)** Representative immunofluorescence images of bone marrow (BM) megakaryocytes (MK) during SARS-CoV-2 infection. Femurs of mice inoculated with SARS-CoV-2 (3 DPI or 7 DPI) or Mock-infected were stained with anti-CD41 (green) and the nuclei counterstained with Hoechst (blue) (scale bar 20 µm). **(B)** MK number was quantified in femurs and expressed as mean (± SD) x mm^{-2} of

tissue. Statistics: one-way ANOVA with Tukey's multiple comparisons, *p < 0.05, n = 3–5 per group. **(C)** Frequency distribution of MK size (diameter in µm, left panel) and area (surface in μm^2 right panel) were analyzed, percentages of frequency are expressed as mean (± SD). Statistics, Two-way ANOVA, Mixed-effects analysis with Tukey's multiple comparisons test; n = 4–5 per group. **(D)** Representative immunofluorescence images of bone marrow or lung during SARS-CoV-2 infection. SARS-CoV-2 was detected using anti-SARS-CoV-2 nucleocapsid (green), and nuclei were counterstained with Hoechst (blue) (scale bar 25 µm). **(E)** Tissues from mice uninfected (Mock) or infected with SARS-CoV-2 for 3 DPI or 7 DPI were analyzed for presence of SARS-CoV-2. Results are expressed as mean (± SD) of SARS-CoV-2 coverage (% of tissue), top panel (dotted line indicates the mean value obtained for mock tissues). Viral RNA levels were determined in bone marrow by RT-ddPCR and compared to those in lungs (bottom panel). SARS-CoV-2 E gene copies were normalized with *Gapdh* mRNA copies (N = 4–5 mice per condition). Results are expressed as mean (± SD). Statistics: Two-way ANOVA, Mixed-effects analysis with Uncorrected Fisher's LSD, *p < 0.05, ****p < 0.0001, n = 3–5 per group.

Figure 3. Spatial transcriptomic analysis of bone marrow megakaryocytes during SARS-CoV-2 infection. Femurs were analysed from K18-hACE2 mice infected with SARS-CoV2 (500 $TCID_{50}$) for 3 days (COVID_3d) or 7 days (COVID_7d) or with conditioned media (Mock) for 7 days. Ten-µm sections of paraffin-embedded femurs were used to perform spatial transcriptomic analysis. **(A)** Schematic illustration of NanoString's GeoMx Digital Spatial Profiler (DSP) workflow. Different steps are indicated: (1) Stain: Femur sections were hybridized with UV photocleavable probes from the whole mouse genome and fluorescent morphology markers. (2) Regions of interest (ROI) were selected based on the fluorescence of interest (CD41) and whether Megakaryocytes (MK) were adjacent to sinusoid vessels (ASV-MK) or non-adjacent to sinusoid vessels (NASV-MK). (3) ROI were illuminated with UV light which released the barcodes. (4) Each ROI was collected independently using microcapillaries. (5) Sequencing libraries were generated followed by sequencing and counting. 19,072 genes normalized by 3rd quartile (Q3) were expressed above LOQ (Limit of Quantitation) in at least 10% of ROI. **(B)** Immunofluorescence staining of bone marrow (femur) using morphology markers. Anti-CD41 antibody (turquoise) was used to stain MK, anti-endomucin antibody (purple) to stain sinusoids and SYTO dye (blue) to stain nuclei. Scale bar 125 µm. Representative ROI (6 to 8 MK per ROI) are illustrated in the right panel. ROI with ASV-MK are yellow, ROI with NASV-MK are white. **(C, D)** Volcano Plots comparing **(C)** COVID-3d or **(D)** COVID-7d versus Mock. The fold change (log2) of each gene is plotted against its statistical significance (-log10 FDR *p* value). Red dots represent genes significantly up-regulated and blue dots genes significantly down-regulated in MK during COVID-19. Thresholds are indicated with dotted lines. **(E)** UMAP (Uniform Manifold Approximation and Projection) plot of the short (30) gene signature of MK-ROI coloured by class (Black circles: Mock (n = 12); red circles: COVID-7d (n

= 12)). **(F)** Heatmap showing differences of the 30-gene signature between Mock and COVID_7d. Each row represents a MK-ROI and each column represents a gene obtained from the short signature. **(G)** Relevant enriched biological processes using the 30-gene signature and their p-values are presented. The 30-gene signature was obtained using a machine learning approach. BioDiscML was used to classified “Mock” and “COVID_7d” groups and the best model was VFI (Variable Feature Importance) optimized with FDR (False Discovery Rate), MCC (Matthew’s Correlation Coefficient) for the model was 0.997. **(H)** PF4 mRNA expression was evaluated in bone barrow by RT-ddPCR. PF4 mRNA copies were normalized with *Gapdh* mRNA copies (N = 4–5 mice per condition). Results are expressed as mean (± SD). Statistics: Unpaired t test with Welch’s correction, *p < 0.05 (n = 4–5 per condition).

Figure 4 Spatial transcriptomic analysis of megakaryocytes within the bone marrow. MK-ROI were selected depending on their position: adjacent to sinusoid vessels (ASV-MK) or non-adjacent to sinusoid vessels (NASV-MK). **(A)** Volcano Plots (Mock ASV-MK (n = 6) versus Mock NASV-MK (n = 6)) shows the fold change (log2) of each gene plotted against its statistical significance (-log10 FDR *p* value). Red dots represent genes significantly up-regulated and blue dots genes significantly down-regulated in megakaryocytes depending on their position. Thresholds are indicated with dotted lines. **(B)** UMAP (Uniform Manifold Approximation and Projection) plot of the short gene signature of MK-ROI coloured by class in Mock condition (Blue circles: Mock ASV (n = 6); red circles: Mock NASV (n = 6)). **(C)** Volcano Plots of COVID-7d ASV-MK (n = 6) versus Mock ASV-MK (n = 6) (left panel) and COVID-7d NASV-MK (n = 6) versus Mock NASV-MK (n=6) (right panel) showing the fold change (log2) of each gene plotted against its statistical significance (-log10 FDR *p* value). Red dots represent genes significantly up-regulated and blue dots genes significantly down-regulated in megakaryocytes during COVID-19. Thresholds are indicated with dotted lines. **(D)** UMAP plot of the short gene signature of MK-ROI coloured by class in Mock ASV-MK (Black circles (n = 6) and COVID_7d ASV-MK red circles (n = 6). **(E)** Volcano Plots (COVID_7d NASV-MK (n = 6) versus Mock NASV-MK (n = 6)) shows the fold change (log2) of each gene plotted against its statistical significance (-log10 FDR *p* value). Red dots represent genes significantly up-regulated and blue dots genes significantly down-regulated in megakaryocytes depending on their position. Thresholds are indicated with dotted lines. **(F)** UMAP plot of the short gene signature of MK-ROI coloured by class in Mock NASV-MK (Black circles (n = 6) and COVID_7d NASV-MK (red circles (n = 6)). **(G)** Heatmap showing differences of the 15-gene signature between ASV-MK in Mock and COVID_7d. Each row represents a MK-ROI and each column represents a gene obtained from the short signature. The 15-gene signature was obtained using a machine learning approach. BioDiscML was used to classified “Mock ASV-MK” and “COVID_7d ASV-MK.” The best model was the Functions Logistic optimized with BER (Balanced Error Rate), MCC for the model was 0.922 ±0.113 **(H)** Heatmap showing differences of the 30-gene signature

between NASV-MK in Mock and COVID_7d. Each row represents a MK-ROI and each column represents a gene obtained from the short signature. The 15-gene signature was obtained using a machine learning approach. BioDiscML was used to classified “Mock NASV-MK” and “COVID_7d NASV-MK.” The best model was the Complement Naïve Bayes with FDR, MCC for the model was 0.922 ±0.114.

References

1. Machlus KR, Italiano JE, Jr. The incredible journey: From megakaryocyte development to platelet formation. *J Cell Biol*. 2013;201(6):785-796.
2. Tilburg J, Becker IC, Italiano JE. Don't you forget about me(gakaryocytes). *Blood*. 2021.
3. Schulze H, Stegner D. Imaging platelet biogenesis in vivo. *Res Pract Thromb Haemost*. 2018;2(3):461-468.
4. Bruns I, Lucas D, Pinho S, et al. Megakaryocytes regulate hematopoietic stem cell quiescence through CXCL4 secretion. *Nat Med*. 2014;20(11):1315-1320.
5. Gong Y, Zhao M, Yang W, et al. Megakaryocyte-derived excessive transforming growth factor beta1 inhibits proliferation of normal hematopoietic stem cells in acute myeloid leukemia. *Exp Hematol*. 2018;60:40-46 e42.
6. Heazlewood SY, Neaves RJ, Williams B, Haylock DN, Adams TE, Nilsson SK. Megakaryocytes co-localise with hemopoietic stem cells and release cytokines that up-regulate stem cell proliferation. *Stem Cell Res*. 2013;11(2):782-792.
7. Koupenova M, Livada AC, Morrell CN. Platelet and Megakaryocyte Roles in Innate and Adaptive Immunity. *Circ Res*. 2022;130(2):288-308.
8. Marcoux G, Laroche A, Espinoza Romero J, Boilard E. Role of platelets and megakaryocytes in adaptive immunity. *Platelets*. 2020:1-12.
9. Beaulieu LM, Lin E, Morin KM, Tanriverdi K, Freedman JE. Regulatory effects of TLR2 on megakaryocytic cell function. *Blood*. 2011;117(22):5963-5974.
10. Zufferey A, Speck ER, Machlus KR, et al. Mature murine megakaryocytes present antigen-MHC class I molecules to T cells and transfer them to platelets. *Blood Adv*. 2017;1(20):1773-1785.
11. Finney BA, Schweighoffer E, Navarro-Nunez L, et al. CLEC-2 and Syk in the megakaryocytic/platelet lineage are essential for development. *Blood*. 2012;119(7):1747-1756.
12. Cunin P, Penke LR, Thon JN, et al. Megakaryocytes compensate for Kit insufficiency in murine arthritis. *J Clin Invest*. 2017;127(5):1714-1724.
13. Chu T, Hu S, Qi J, et al. Bifunctional effect of the inflammatory cytokine tumor necrosis factor alpha on megakaryopoiesis and platelet production. *J Thromb Haemost*. 2022;20(12):2998-3010.
14. Beaulieu LM, Lin E, Mick E, et al. Interleukin 1 receptor 1 and interleukin 1beta regulate megakaryocyte maturation, platelet activation, and transcript profile during inflammation in mice and humans. *Arterioscler Thromb Vasc Biol*. 2014;34(3):552-564.

15. Ajanel A, Middleton EA. Alterations in the megakaryocyte transcriptome impacts platelet function in sepsis and COVID-19 infection. *Thromb Res*. 2023.
16. Middleton EA, Rowley JW, Campbell RA, et al. Sepsis alters the transcriptional and translational landscape of human and murine platelets. *Blood*. 2019;134(12):911-923.
17. Campbell RA, Schwertz H, Hottz ED, et al. Human megakaryocytes possess intrinsic antiviral immunity through regulated induction of IFITM3. *Blood*. 2019;133(19):2013-2026.
18. Lood C, Amisten S, Gullstrand B, et al. Platelet transcriptional profile and protein expression in patients with systemic lupus erythematosus: up-regulation of the type I interferon system is strongly associated with vascular disease. *Blood*. 2010;116(11):1951-1957.
19. Melki I, Allaeys I, Tessandier N, et al. FcgammaRIIA expression accelerates nephritis and increases platelet activation in systemic lupus erythematosus. *Blood*. 2020;136(25):2933-2945.
20. Cornwell MG, Bannoudi HE, Luttrell-Williams E, et al. Modeling of clinical phenotypes in systemic lupus erythematosus based on the platelet transcriptome and FCGR2a genotype. *J Transl Med*. 2023;21(1):247.
21. Sun S, Jin C, Si J, et al. Single-cell analysis of ploidy and the transcriptome reveals functional and spatial divergency in murine megakaryopoiesis. *Blood*. 2021;138(14):1211-1224.
22. Puhm F, Laroche A, Boilard E. Diversity of Megakaryocytes. *Arterioscler Thromb Vasc Biol*. 2023.
23. Levine RF, Eldor A, Shoff PK, Kirwin S, Tenza D, Cramer EM. Circulating megakaryocytes: delivery of large numbers of intact, mature megakaryocytes to the lungs. *Eur J Haematol*. 1993;51(4):233-246.
24. Lefrancais E, Ortiz-Munoz G, Caudrillier A, et al. The lung is a site of platelet biogenesis and a reservoir for haematopoietic progenitors. *Nature*. 2017;544(7648):105-109.
25. Pariser DN, Hilt ZT, Ture SK, et al. Lung megakaryocytes are immune modulatory cells. *J Clin Invest*. 2021;131(1).
26. Valet C, Magnen M, Qiu L, et al. Sepsis promotes splenic production of a protective platelet pool with high CD40 ligand expression. *J Clin Invest*. 2022;132(7).
27. Bonaventura A, Vecchie A, Dagna L, et al. Endothelial dysfunction and immunothrombosis as key pathogenic mechanisms in COVID-19. *Nat Rev Immunol*. 2021;21(5):319-329.
28. Conway EM, Mackman N, Warren RQ, et al. Understanding COVID-19-associated coagulopathy. *Nat Rev Immunol*. 2022;22(10):639-649.
29. Zaid Y, Puhm F, Allaeys I, et al. Platelets Can Associate with SARS-Cov-2 RNA and Are Hyperactivated in COVID-19. *Circ Res*. 2020;127(11):1404-1418.
30. Manne BK, Denorme F, Middleton EA, et al. Platelet gene expression and function in patients with COVID-19. *Blood*. 2020;136(11):1317-1329.
31. Hottz ED, Azevedo-Quintanilha IG, Palhinha L, et al. Platelet activation and platelet-monocyte aggregates formation trigger tissue factor expression in severe COVID-19 patients. *Blood*. 2020.

32. Fortmann SD, Patton M, Frey BF, et al. Circulating SARS-CoV-2+ Megakaryocytes Associate with Severe Viral Infection in COVID-19. *Blood Adv*. 2023.
33. Ren X, Wen W, Fan X, et al. COVID-19 immune features revealed by a large-scale single-cell transcriptome atlas. *Cell*. 2021;184(7):1895-1913 e1819.
34. Gough PJ, Gomez IG, Wille PT, Raines EW. Macrophage expression of active MMP-9 induces acute plaque disruption in apoE-deficient mice. *J Clin Invest*. 2006;116(1):59-69.
35. Carstairs KC. The identification of platelets and platelet antigens in histological sections. *J Pathol Bacteriol*. 1965;90(1):225-231.
36. Rendeiro AF, Ravichandran H, Bram Y, et al. The spatial landscape of lung pathology during COVID-19 progression. *Nature*. 2021;593(7860):564-569.
37. Leclercq M, Vittrant B, Martin-Magniette ML, et al. Large-Scale Automatic Feature Selection for Biomarker Discovery in High-Dimensional OMICs Data. *Front Genet*. 2019;10:452.
38. Raudvere U, Kolberg L, Kuzmin I, et al. g:Profiler: a web server for functional enrichment analysis and conversions of gene lists (2019 update). *Nucleic Acids Res*. 2019;47(W1):W191-W198.
39. McCray PB, Jr., Pewe L, Wohlford-Lenane C, et al. Lethal infection of K18-hACE2 mice infected with severe acute respiratory syndrome coronavirus. *J Virol*. 2007;81(2):813-821.
40. Dubuc I, Prunier J, Lacasse E, et al. Cytokines and Lipid Mediators of Inflammation in Lungs of SARS-CoV-2 Infected Mice. *Front Immunol*. 2022;13:893792.
41. Zaid Y, Dore E, Dubuc I, et al. Chemokines and eicosanoids fuel the hyperinflammation within the lungs of patients with severe COVID-19. *J Allergy Clin Immunol*. 2021;148(2):368-380 e363.
42. Barrett TJ, Cornwell M, Myndzar K, et al. Platelets amplify endotheliopathy in COVID-19. *Sci Adv*. 2021;7(37):eabh2434.
43. Tilburg J, Stone AP, Billingsley JM, et al. Spatial transcriptomics of murine bone marrow megakaryocytes at single-cell resolution. *Res Pract Thromb Haemost*. 2023;7(4):100158.
44. Vargas ESCF, Nguyen R, Willson M, et al. Intravital imaging of 3 different microvascular beds in SARS-CoV-2-infected mice. *Blood Adv*. 2023.
45. Comer SP, Cullivan S, Szklanna PB, et al. COVID-19 induces a hyperactive phenotype in circulating platelets. *PLoS Biol*. 2021;19(2):e3001109.
46. Hermesh T, Moltedo B, Moran TM, Lopez CB. Antiviral instruction of bone marrow leukocytes during respiratory viral infections. *Cell Host Microbe*. 2010;7(5):343-353.
47. Rommel MGE, Walz L, Fotopoulou F, et al. Influenza A virus infection instructs hematopoiesis to megakaryocyte-lineage output. *Cell Rep*. 2022;41(1):111447.
48. Stein SR, Ramelli SC, Grazioli A, et al. SARS-CoV-2 infection and persistence in the human body and brain at autopsy. *Nature*. 2022;612(7941):758-763.

49. Lamers MM, Haagmans BL. SARS-CoV-2 pathogenesis. *Nat Rev Microbiol*. 2022;20(5):270-284.
50. Khaddaj-Mallat R, Aldib N, Bernard M, et al. SARS-CoV-2 deregulates the vascular and immune functions of brain pericytes via Spike protein. *Neurobiol Dis*. 2021;161:105561.
51. Ma X, Guan C, Chen R, et al. Pathological and molecular examinations of postmortem testis biopsies reveal SARS-CoV-2 infection in the testis and spermatogenesis damage in COVID-19 patients. *Cell Mol Immunol*. 2021;18(2):487-489.
52. Xia H, Cao Z, Xie X, et al. Evasion of Type I Interferon by SARS-CoV-2. *Cell Rep*. 2020;33(1):108234.
53. Machlus KR, Johnson KE, Kulenthirarajan R, et al. CCL5 derived from platelets increases megakaryocyte proplatelet formation. *Blood*. 2016;127(7):921-926.
54. Paludan SR, Mogensen TH. Innate immunological pathways in COVID-19 pathogenesis. *Sci Immunol*. 2022;7(67):eabm5505.
55. Vogl T, Tenbrock K, Ludwig S, et al. Mrp8 and Mrp14 are endogenous activators of Toll-like receptor 4, promoting lethal, endotoxin-induced shock. *Nat Med*. 2007;13(9):1042-1049.
56. Puhm F, Flamand L, Boilard E. Platelet extracellular vesicles in COVID-19: Potential markers and makers. *J Leukoc Biol*. 2022;111(1):63-74.
57. French SL, Butov KR, Allaeys I, et al. Platelet-derived extracellular vesicles infiltrate and modify the bone marrow during inflammation. *Blood Adv*. 2020;4(13):3011-3023.
58. Puhm F, Allaeys I, Lacasse E, et al. Platelet activation by SARS-CoV-2 implicates the release of active tissue factor by infected cells. *Blood Adv*. 2022;6(12):3593-3605.
59. Kim OV, Litvinov RI, Gagne AL, French DL, Brass LF, Weisel JW. Megakaryocyte-induced contraction of plasma clots: cellular mechanisms and structural mechanobiology. *Blood*. 2024;143(6):548-560.
60. Sciaudone A, Corkrey H, Humphries F, Koupenova M. Platelets and SARS-CoV-2 During COVID-19: Immunity, Thrombosis, and Beyond. *Circ Res*. 2023;132(10):1272-1289.
61. Campbell RA, Boilard E, Rondina MT. Is there a role for the ACE2 receptor in SARS-CoV-2 interactions with platelets? *J Thromb Haemost*. 2021;19(1):46-50.
62. Maugeri N, De Lorenzo R, Clementi N, et al. Unconventional CD147-dependent platelet activation elicited by SARS-CoV-2 in COVID-19. *J Thromb Haemost*. 2022;20(2):434-448.
63. Barrett TJ, Bilaloglu S, Cornwell M, et al. Platelets contribute to disease severity in COVID-19. *J Thromb Haemost*. 2021;19(12):3139-3153.
64. Zhu A, Real F, Capron C, et al. Infection of lung megakaryocytes and platelets by SARS-CoV-2 anticipate fatal COVID-19. *Cell Mol Life Sci*. 2022;79(7):365.
65. Koupenova M, Corkrey HA, Vitseva O, et al. SARS-CoV-2 Initiates Programmed Cell Death in Platelets. *Circ Res*. 2021;129(6):631-646.

66. Garcia C, Au Duong J, Poette M, et al. Platelet activation and partial desensitization are associated with viral xenophagy in patients with severe COVID-19. *Blood Adv*. 2022;6(13):3884-3898.
67. Zhao X, Alibhai D, Walsh TG, et al. Highly efficient platelet generation in lung vasculature reproduced by microfluidics. *Nat Commun*. 2023;14(1):4026.
68. Yeung AK, Villacorta-Martin C, Hon S, Rock JR, Murphy GJ. Lung megakaryocytes display distinct transcriptional and phenotypic properties. *Blood Adv*. 2020;4(24):6204-6217.
69. Cunin P, Bouslama R, Machlus KR, et al. Megakaryocyte emperipolesis mediates membrane transfer from intracytoplasmic neutrophils to platelets. *Elife*. 2019;8.
70. Cunin P, Nigrovic PA. Megakaryocyte emperipolesis: a new frontier in cell-in-cell interaction. *Platelets*. 2020;31(6):700-706.
71. Stegner D, vanEeuwijk JMM, Angay O, et al. Thrombopoiesis is spatially regulated by the bone marrow vasculature. *Nat Commun*. 2017;8(1):127.

Figure 1

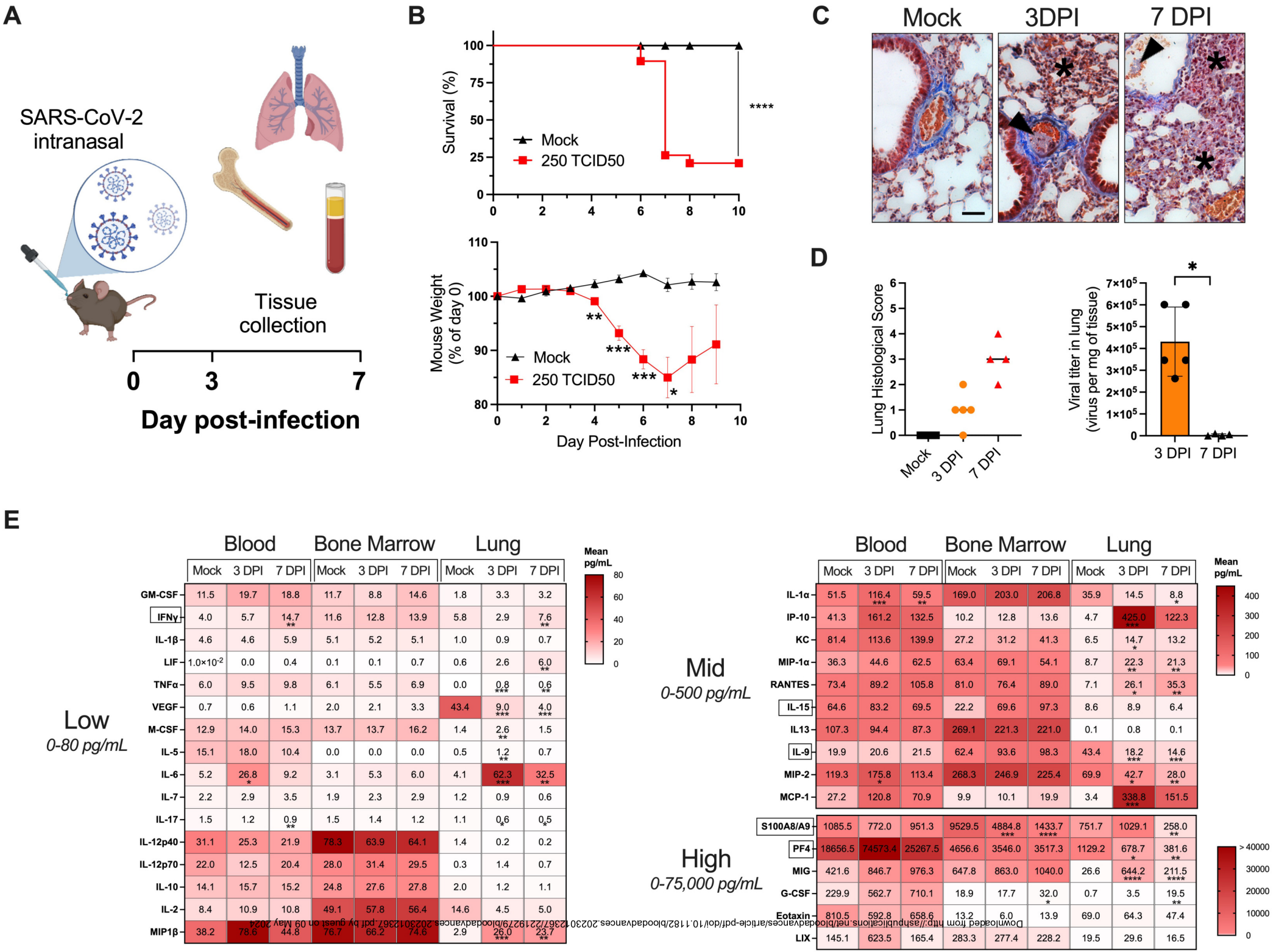

	Blood			Bone Marrow			Lung		
	Mock	3 DPI	7 DPI	Mock	3 DPI	7 DPI	Mock	3 DPI	7 DPI
GM-CSF	11.5	19.7	18.8	11.7	8.8	14.6	1.8	3.3	3.2
IFNγ	4.0	5.7	14.7 **	11.6	12.8	13.9	5.8	2.9	7.6 **
IL-1β	4.6	4.6	5.9	5.1	5.2	5.1	1.0	0.9	0.7
LIF	1.0×10^{-2}	0.0	0.4	0.1	0.1	0.7	0.6	2.6	6.0 **
TNFα	6.0	9.5	9.8	6.1	5.5	6.9	0.0	0.8 ***	0.6 **
VEGF	0.7	0.6	1.1	2.0	2.1	3.3	43.4	9.0 ***	4.0 ***
M-CSF	12.9	14.0	15.3	13.7	13.7	16.2	1.4	2.6 **	1.5
IL-5	15.1	18.0	10.4	0.0	0.0	0.0	0.5	1.2 **	0.7
IL-6	5.2	26.8 *	9.2	3.1	5.3	6.0	4.1	62.3 ***	32.5 **
IL-7	2.2	2.9	3.5	1.9	2.3	2.9	1.2	0.9	0.6
IL-17	1.5	1.2	0.9 **	1.5	1.4	1.2	1.1	0.6 *	0.5 *
IL-12p40	31.1	25.3	21.9	78.3	63.9	64.1	1.4	0.2	0.2
IL-12p70	22.0	12.5	20.4	28.0	31.4	29.5	0.3	1.4	0.7
IL-10	14.1	15.7	15.2	24.8	27.6	27.8	2.0	1.2	1.1
IL-2	8.4	10.9	10.8	49.1	57.8	56.4	14.6	4.5	5.0
MIP1β	38.2	78.6	44.8	76.7	66.2	74.6	2.9	26.0 ***	23.7 **

	Blood			Bone Marrow			Lung		
	Mock	3 DPI	7 DPI	Mock	3 DPI	7 DPI	Mock	3 DPI	7 DPI
IL-1α	51.5	116.4 ***	59.5 **	169.0	203.0	206.8	35.9	14.5	8.8 *
IP-10	41.3	161.2	132.5	10.2	12.8	13.6	4.7	425.0 ***	122.3
KC	81.4	113.6	139.9	27.2	31.2	41.3	6.5	14.7 *	13.2
MIP-1α	36.3	44.6	62.5	63.4	69.1	54.1	8.7	22.3 **	21.3 **
RANTES	73.4	89.2	105.8	81.0	76.4	89.0	7.1	26.1 *	35.3 **
IL-15	64.6	83.2	69.5	22.2	69.6	97.3	8.6	8.9	6.4
IL13	107.3	94.4	87.3	269.1	221.3	221.0	0.1	0.8	0.1
IL-9	19.9	20.6	21.5	62.4	93.6	98.3	43.4	18.2 ***	14.6 ***
MIP-2	119.3	175.8 *	113.4	268.3	246.9	225.4	69.9	42.7 *	28.0 **
MCP-1	27.2	120.8	70.9	9.9	10.1	19.9	3.4	338.8 ***	151.5
S100A8/A9	1085.5	772.0	951.3	9529.5	4884.8 ***	1433.7 ****	751.7	1029.1	258.0 **
PF4	18656.5	74573.4	25267.5	4656.6	3546.0	3517.3	1129.2	678.7 *	381.6 **
MIG	421.6	846.7	976.3	647.8	863.0	1040.0	26.6	644.2 ****	211.5 ****
G-CSF	229.9	562.7	710.1	18.9	17.7	32.0 *	0.7	3.5	19.5 **
Eotaxin	810.5	592.8	658.6	13.2	6.0	13.9	69.0	64.3	47.4
LIX	145.1	623.5	165.4	283.3	277.4	228.2	19.5	29.6	16.5

Figure 2

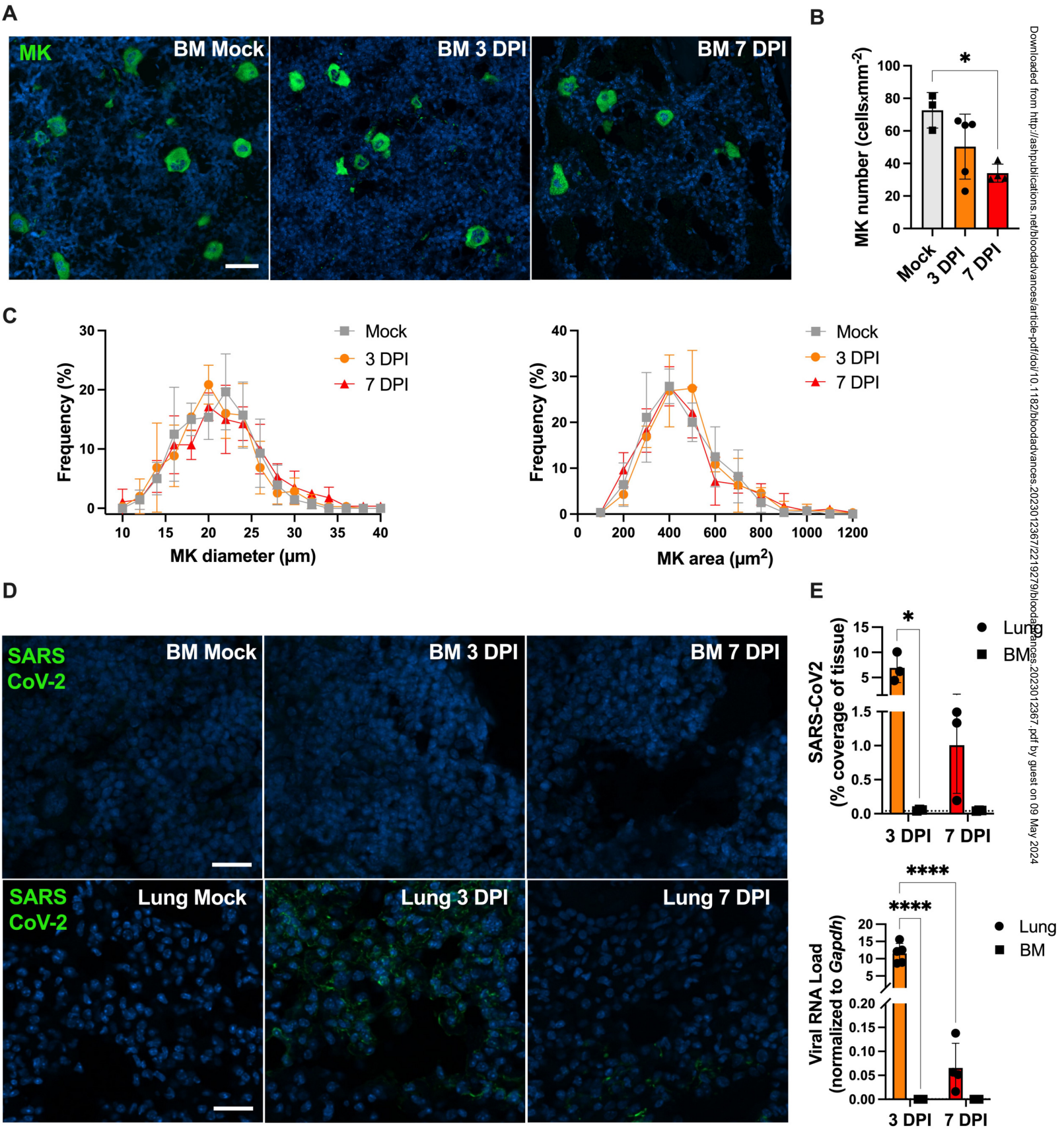

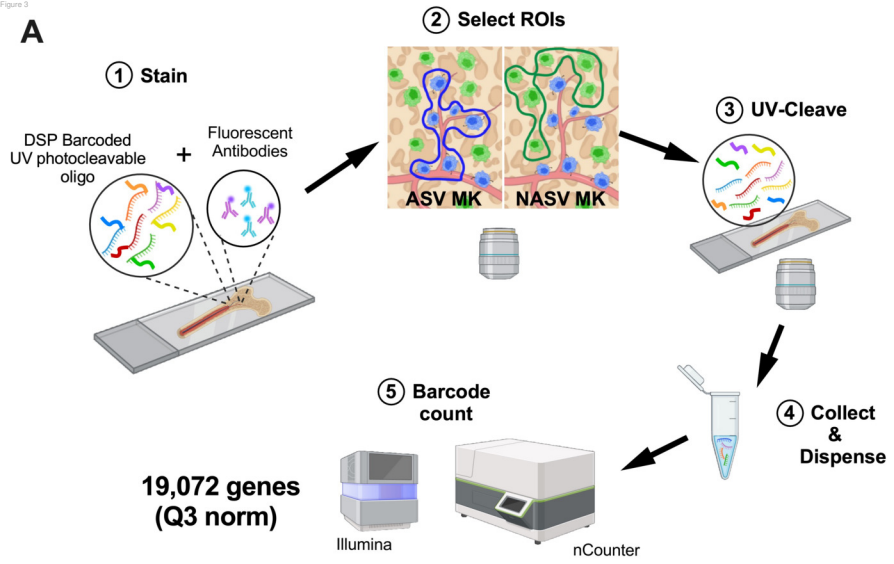

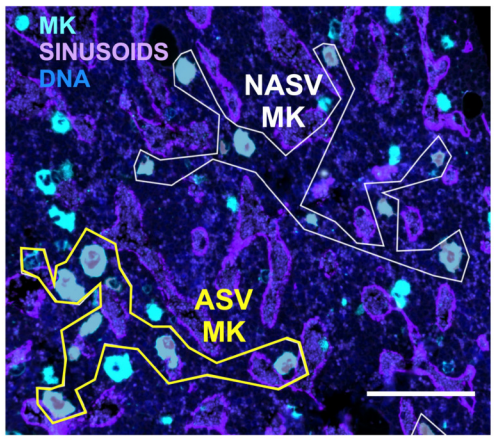

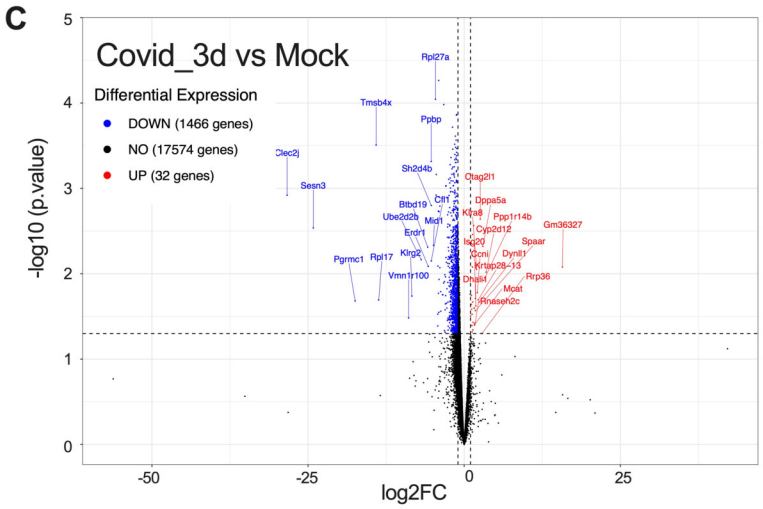

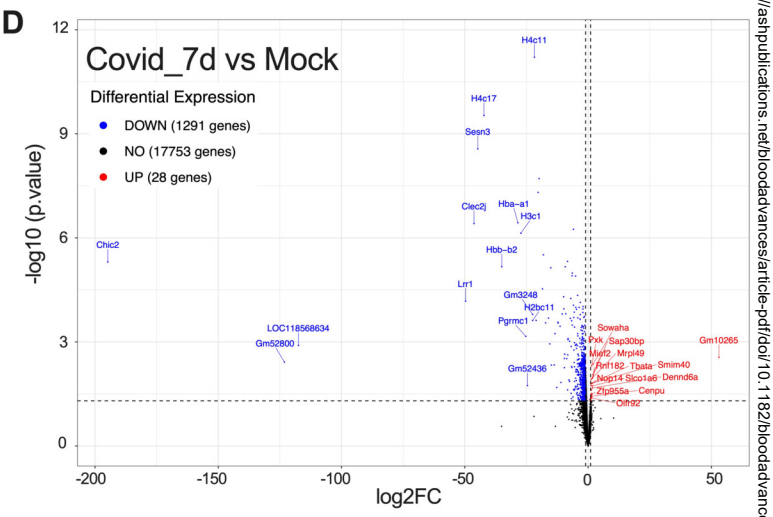

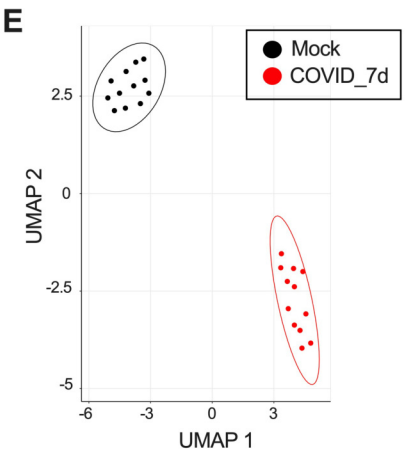

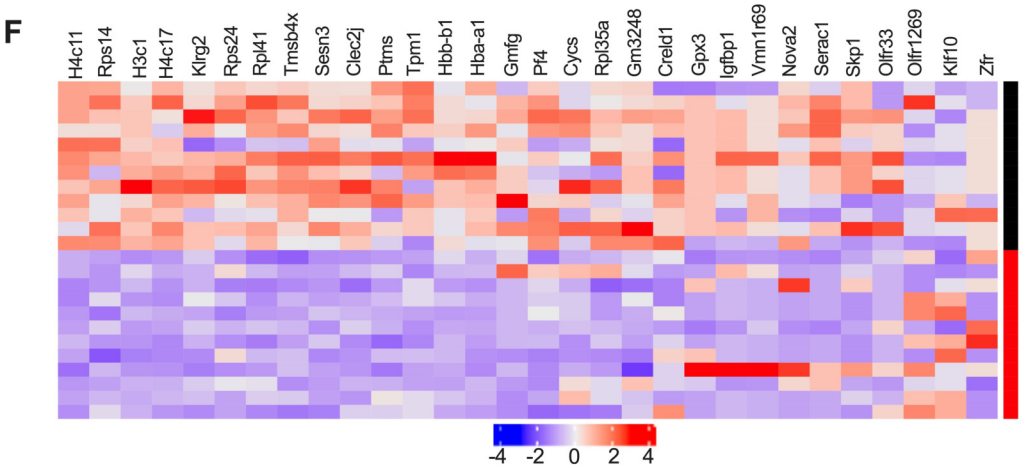

G

Enriched Biological Processes	Associated genes	P-value
KEGG		
Ribosome	Rpl35a, Rpl41, Rps14, Rps24	7.633e-5
Coronavirus disease - COVID-19	Rpl35a, Rpl41, Rps14, Rps24	3.165e-4
Systemic Lupus Erythematosus	H3c1, H3c11, H4c17	2.607e-3
Neutrophil Extracellular Trap formation	H3c1, H3c11, H4c17	7.208e-3
REAC		
HDMs demethylate histones	H3c1, H3c11, H4c17	2.105e-4
PKMTs methylate histones lysines	H3c1, H3c11, H4c17	5.855e-4
RMTs methylates histones arginines	H3c1, H3c11, H4c17	7.377e-4
HATs Acethylate histones	H3c1, H3c11, H4c17	9.140e-4
Metabolism of proteins	H3c11, H4c17, Igfbp1, Rpl35a, Rps14, Rps24, Skp1	4.985e-4
PRC2 methylates histones and DNA	H3c1, H3c11, H4c17	1.251e-3
RUNX1 regulates genes involved in megakaryocytes differentiation and platelet function	H3c1, H3c11, H4c17	1.551e-3
Detoxification of Reactive Oxygen Species	Cycs, Gpx3	1.518e-2

H